Infrared Spectra of Indium Hydrides in Solid Hydrogen and Neon

Xuefeng Wang and Lester Andrews*

Department of Chemistry, University of Virginia, McCormick Road, P.O. Box 400319, Charlottesville, Virginia 22904-4319

Received: December 19, 2003; In Final Form: February 17, 2004

Reactions of laser-ablated In atoms with pure hydrogen and pure deuterium give sharp absorptions for the InH and InD intermediate species. Ultraviolet irradiation produces InH_2 and InD_2 and maximizes the yield of the indane monomers InH_3 and InD_3, which are observed as the hypervalent complexes $(H_2)InH_3$ and $(D_2)InD_3$. In addition $In^+(H_2)_n$ and $In^+(D_2)_n$ cations and $H^-(H_2)_n$ and $D^-(D_2)_n$ anions are observed in these samples. Irradiation at 193 nm photoionizes In, increases the yields of both cation and ion, excites In to activate the endothermic reaction with H_2 to form InH, and promotes the conversion of InH to InH_3. Annealing to 6−8 K provides evidence for In_2H_2, In_2D_2, In_2H_4, and In_2D_4 isomers, In_2H_6, and In_2D_6, and warming the samples to allow evaporation of the H_2 and D_2 matrix hosts replaces the sharp absorptions by broad 1460 and 1060 cm^{-1} bands with dominant contributions from solid indane $(InH_3)_n$ and $(InD_3)_n$, respectively. Diindane is unstable on ultraviolet photolysis in contrast to digallane and dialane. Our solid indane sample decomposes at 180−190 K, which casts doubt on earlier reports for its preparation. Complementary neon matrix experiments give smaller yields of InH_{1-3} and larger yields of In_2H_2 and InH_4^- than solid hydrogen experiments.

Introduction

Indane and thallane have been controversial compounds. Claims for the early preparation of solid $(InH_3)_n$ and $(TlH_3)_n$ by Wiberg[1,2] have been rejected by subsequent workers. Mass spectroscopic investigation of the comparative stabilities of AlH_3, GaH_3, and InH_3 cast doubt on the stability of $(InH_3)_n$ claimed by Wiberg.[3] Attempts to reproduce the Wiberg preparation of indane and thallane have failed,[4] and review papers do not list these compounds.[5,6] Theoretical investigations conclude that solid indane and thallane do not have the room temperature stability reported for the previous solid materials.[7] Despite their anticipated instability, InH_3 complexes prepared from the $LiInH_4$ reagent[8] are stabilized through interaction with a strong and bulky base.[9−11]

In contrast spectroscopic evidence for the InH, InH_2, and InH_3 molecules is available. The diatomic molecule has been investigated at high resolution in the gas phase and in solid argon.[12−20] The dihydride radical and trihydride monomer have been thoroughly characterized in combined matrix isolation and theoretical investigations: Both are analogous to the Al and Ga counterparts.[19,20] Electronic structure and bond strengths have been computed for the InH_x species.[21−23]

We recently reported the preparation of dialane and solid alane using the reaction of laser-ablated Al with pure H_2 during condensation at 3.5 K.[24,25] The reaction first formed AlH, and then UV photolysis and annealing gave AlH_3 and Al_2H_6 in solid hydrogen. After evaporation of the H_2 matrix host, a solid alane film remained on the CsI window until it was removed by cleaning at room temperature. This film exhibited broad IR absorptions at 1720 and 720 cm^{-1}, which are almost identical to the 1760 and 680 cm^{-1} bands reported for solid $(AlH_3)_n$ samples that involve Al−H−Al bridge bonds in a network solid.[26,27] Complementary experiments with thermal Al atoms and UV photolysis gave the same AlH_{1-3} and $Al_2H_{2,4,6}$ hydride species.[25] Similar experiments with laser-ablated Ga in pure H_2 give GaH, GaH_2, and GaH_3 absorptions, and UV photolysis and annealing produced weak Ga_2H_6 absorptions.[28] After the H_2 matrix evaporated, a broad absorption with peaks at 1870 and 1600−1400 cm^{-1} remained until the window reached 240 K. These broad bands compare favorably with features in the spectrum of solid gallane oligomers formed by condensing the prepared material, which evaporate digallane on warming to 210 K.[29,30] We also describe the preparation of solid $(InH_3)_n$ using the same methods: A preliminary communication on this indium hydride work has been published.[31]

Experimental and Theoretical Methods

The laser ablation matrix isolation infrared spectroscopy experiment has been described previously.[32] Briefly, the Nd:YAG laser fundamental (1064 nm, 10 Hz repetition rate, 10 ns pulse width) was focused on a rotating high purity-indium target (Indium Corporation of America) using 1−5 mJ/pulse, and atoms were codeposited with pure H_2 or D_2 (Matheson) or HD (Cambridge Isotope Laboratories) onto a CsI window cooled to 3.5 K by a Sumitomo Heavy Industries RDK-205D cryocooler. Infrared spectra were recorded by a Nicolet 750 Fourier transform instrument at 0.5 cm^{-1} resolution using a liquid-nitrogen-cooled HgCdTe detector after deposition, annealing, and filtered UV−vis mercury arc (175 W) or unfocused 193 nm argon fluoride laser irradiation (Lambda Physik, 2−4 mJ/pulse at 10 Hz). We annealed solid hydrogen samples to 6.0−7.0 K using resistance heat on the refrigerator cold stage: The samples were held above 6 K for less than 30 s, and a neon overcoat was employed to limit evaporation of the matrix. Emission spectra were recorded during ablation and for 193 nm excitation using an Ocean Optics USB2000 optical fiber spectrometer system.

Density functional theory (DFT) frequency calculations were helpful in assigning lead and platinum hydride spectra,[33,34] so

* To whom correspondence should be addressed. E-mail: lsa@virginia.edu.

10.1021/jp037942l CCC: $27.50
Published on Web 04/24/2004

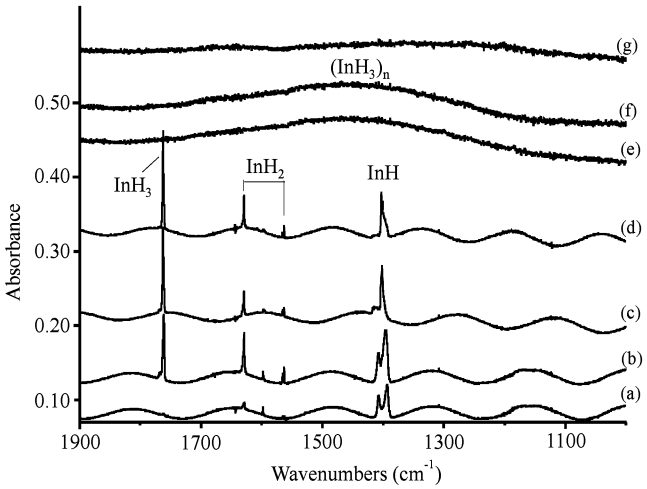

Figure 1. Infrared spectra in the 1900−1000 cm^{-1} region for laser-ablated In codeposited with pure normal isotopic hydrogen at 3.5 K: (a) pure H_2 and In deposited. (b) after 193 nm irradiation for 3 min, (c) after 193 nm irradiation for 58 min (total), (d) after annealing to 6.2 K, (e) after annealing to 8 K, (f) spectrum recorded at 70−100 K, and (g) spectrum recorded at 180−200 K.

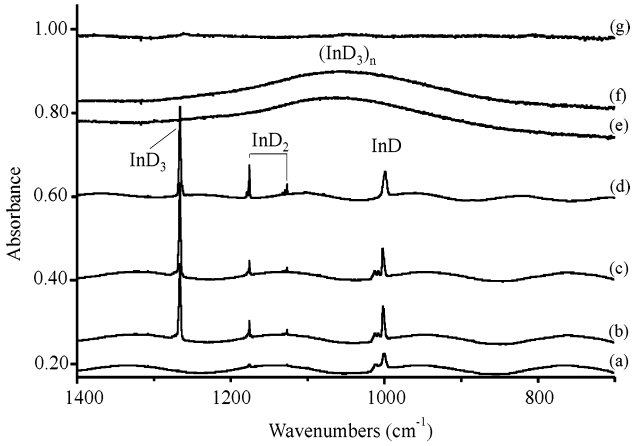

Figure 2. Infrared spectra in the 1400−700 cm^{-1} region for laser-ablated In codeposited with pure D_2 at 3.5 K: (a) pure D_2 and In deposited, (b) after 193 nm irradiation for 20 min, (c) after 193 nm irradiation for 40 min (total), (d) after annealing to 9.0 K, (e) spectrum recorded at 30−60 K, (f) spectrum recorded at 110−130 K, and (g) spectrum recorded at 200−220 K.

similar B3LYP/6-311++G(d,p)/LANL2DZ calculations were performed for indium hydrides.[35−38] Comparable results were obtained using the BPW91 functional.[39] Although these calculations are only approximate, they provide a useful guide for assigning vibrational spectra.

Results and Discussion

Laser ablation of indium gives a purple emission, and codeposition with pure normal hydrogen as a matrix and reagent yields new reaction products, which will be identified from infrared spectra and DFT calculations.

$InH_{1,2,3}$. Infrared spectra are illustrated for laser-ablated In codeposition with pure H_2 and with pure D_2 in Figures 1 and 2. The strong absorptions at 1393.4 and 999.7 cm^{-1} in the deposited sample are between the gas-phase (1424.8 and 1023.5 cm^{-1})[15−18] and solid argon (1387.4 and 995.9 cm^{-1})[19,20] fundamentals for InH and InD, which indicates like assignments in solid H_2 and solid D_2. Ultraviolet irradiation increases the InH and InD absorptions, and the 1628.9 and 1563.3 cm^{-1} and 1175.2 and 1126.3 cm^{-1} band pairs, which are assigned to InH_2 and InD_2 as these bands are 13−15 cm^{-1} higher than the documented argon matrix observations.[19] Further UV irradiation increases new bands at 1760.9 and 1266.2 cm^{-1}, which are due to InH_3 and InD_3 in solid H_2 and solid D_2 as they appear slightly higher than the 1754.5 and 1261.2 cm^{-1} argon matrix bands.[20] Additional associated 615.3 and 609.1 cm^{-1} and 441.1 and 433.0 cm^{-1} bands are also due to InH_3 and InD_3, respectively. Irradiation at 193 nm was particularly effective for producing InH_3 and InD_3. Counterparts for these absorptions were also observed in solid HD (Figure 3). The initial reaction gave InH, InD, and InHD, but photolysis and annealing favored increased yields of InH_2 and InD_2. Very weak absorptions ($A = 0.001$) were observed for In_2O at 737.2 cm^{-1} and for HInOH at 1495.7 cm^{-1} in some experiments: These species have been observed at 735.2 and 1486.3 cm^{-1} in solid argon, respectively.[40,41] New product absorptions are collected in Table 1. Note that the frequencies vary slightly between solid H_2 and HD, and between HD and D_2, because the solid host is a different medium. The sharp H_2O absorption is 1598.1, 1594.8, and 1597.2 cm^{-1} in solid H_2, HD, and D_2, respectively.

We present new observations here for the diffusion and reaction of H atoms in the solid hydrogen matrix at 3.5 K. A sharp, new 4143.4 cm^{-1} absorption due to trapped H atoms

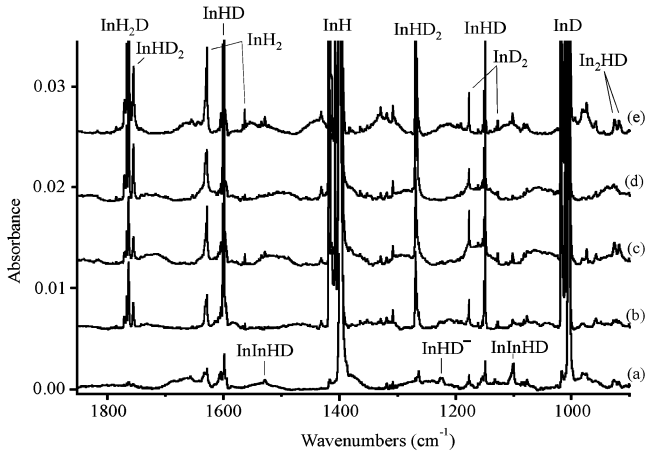

Figure 3. Infrared spectra in the 1800−900 cm^{-1} region for laser-ablated In codeposited with pure HD at 3.5 K: (a) pure HD and In deposited, (b) after $\lambda > 240$ nm irradiation for 15 min, (c) after annealing to 7.6 K, (d) after $\lambda > 240$ nm irradiation, and (e) after annealing to 7.8 K.

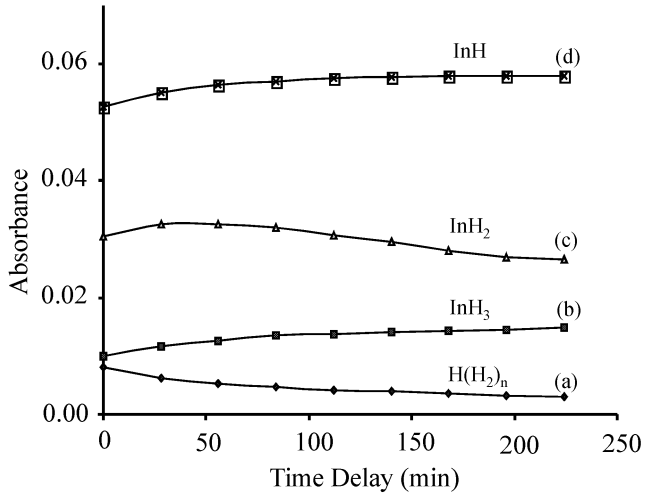

Figure 4. Absorbance (integrated AU × cm^{-1}) vs time delay (min) plots for product absorptions in the solid H_2 sample maintained at 3.5 K: (a) $H(H_2)_n$, (b) InH_3, (c) InH_2, and (d) InH (multiply given absorbance scale × 10 for InH).

TABLE 1: Infrared Absorptions (cm^{-1}) Observed from Reaction of Indium and Dihydrogen in Neon and Pure Hydrogen[a]

neon[b]			hydrogen			
H_2	HD	D_2	H_2	HD	D_2	identification
			4113.1		2961.8	$In^+(H_2)_n$
			4111.7		2959.6	$In^+(H_2)_n$ site
			4098.5		2947.5, 2945.5	$(H_2)InH_3$
1766			1760.9	1766.9, 1763.4, 1754.9		InH_3
		1269		1268.5, 1265.8	1266.2	InD_3
			1707.0			In_2H_4
			1703.6			In_2H_4
			1630.7	1631.8		InH_2 (site)
1636	1605		1628.9	1628.8		InH_2
				1600.7		InHD (site)
				1598.5		InHD
		1180		1178.8	1176.2	InD_2 (site)
				1175.9	1175.2	InD_2
				1150.3		InHD (site)
1613		1161	1607.8		1151.6	$(InH_4^-)^c$
				1148.4		InHD
			1565.4	1566.1		InH_2 (site)
1570	1154		1563.3	1563.3		InH_2
				1128.5	1128.7	InD_2 (site)
		1132		1126.5	1126.3	InD_2
			1529.9	1533.5		$InInH_2$
1537.3	1534.9		1527.5	1528.7		$InInH_2$
	1107.0	1104.6		1101.3	1102.9	$InInD_2$
					1098.8	$InInD_2$
			628.7		456.0	$InInH_2$
			1407.9	1407.4		InH (site)
1409	1408		1393.4	1399.8		InH
				1010.6	1011.3	InD (site)
	1010	1009		1005.2	999.7	InD
1234	1236		1225	1227		$(InH_2^-)^c$
	893	893		884	883	$(InD_2^-)^c$
982.6			979.6	917.7		In_2H_2
	923.3					In_2HD
	647.1	711.7			709.9	In_2D_2
			760.2	761.5		$In(H)_3InH$ (2)
746	745		753.3	752.7, 746.8	551.2	$In(H)_3InH$ (2)
742	741	552	748.1		543.4	$In(H)_3InH$ (2)
			615.3	605.7		InH_3
				553.8	441.1	InD_3
			609.1	535.3		InH_3
				434.2	433.0	InD_3

[a] Absorptions for In_2H_4 and In_2H_6 are presented in Tables 3 and 4. Sharper bands with 1−2 cm^{-1} widths are accurate to ±0.2 cm^{-1}. [b] Broader bands with 5−10 cm^{-1} widths are accurate to ±1 cm^{-1}. [c] Tentative assignments.

($H(H_2)_n$) decreases with delay time, while InH increases, InH_2 increases and then decreases, and finally InH_3 increases. At this low temperature H atoms are the diffusing reagent, and sequential H atom reactions with In atoms form InH, InH_2, and InH_3. Figure 4 illustrates the absorbance−time plots for these hydride species.

Experiments were done with *p*-enriched hydrogen, and in a 99% *p*-H_2 sample the product absorptions were observed at 4119.7, 1762.5, 1629.2, 1563.5, 1416.4, and 1403.4 cm^{-1}. The $InH_{1,2,3}$ absorptions are blue shifted 1.6, 0.3 (0.2), and 10.0 cm^{-1}, respectively, compared to *n*-H_2. In a 98% *o*-D_2 sample the product absorptions were 2961.9, 1266.4, 1175.4, 1126.4, and 1001.6 cm^{-1}. The $InD_{1,2,3}$ absorptions are blue shifted 0.2, 0.2 (0.1), and 1.9 cm^{-1}, respectively, compared to *n*-D_2.

Counterparts of these $InH_{1,2,3}$ absorptions are observed in solid neon as illustrated in Figure 5. The neon matrix counterparts are 16 cm^{-1} (InH), 7 and 7 cm^{-1} (InH_2), and 5 cm^{-1} (InH_3) higher than the *n*-H_2 matrix values, which are in turn 6.0, 13.3, 14.7, and 6.4 cm^{-1} higher, respectively, than argon matrix frequencies.[19,20] This and the Manceron argon matrix study[19,20] are the only experimental work on the InH_2 and InH_3 transients. Several differences are noteworthy: The overall indium hydride yield is much less in neon than in solid hydrogen, particularly so for InH_3, but the yield of InH dimer, namely, In_2H_2, at 979.6 cm^{-1}, based on the 954.8 cm^{-1} argon matrix assignment,[42] is much larger. The H_2 and Ne matrix shifts for InH_{1-3} from argon are small, and the Ne matrix observations give a better prediction of gas-phase values.

To provide support for identification of new indium hydride species, DFT isotopic frequency calculations were performed using B3LYP and BPW91 functionals and the small LANL2DZ pseudopotential and basis for In. The higher B3LYP frequencies fit better: Taking the neon matrix frequencies for comparison, the computed In−H stretching frequencies are 0.2% low, 0.0 and 1.7% high, and 1.1% high for the three InH_{1-3} hydrides, respectively. Table 2 gives the B3LYP frequencies for comparison with other indium hydride species.

$(H_2)InH_3$. A sharp absorption is produced on UV irradiation at 4098.5 [2947.5] cm^{-1} in solid hydrogen [deuterium] (Figure 6) along with the strong 1790.0 [1266.2] cm^{-1} band for InH_3 [InD_3]. These H−H [D−D] stretching bands (H_2/D_2 ratio 1.3905) are red-shifted 54.3 [39.3] cm^{-1} from the solid hydrogen [deuterium] mode observed at 4152.8 [2986.8] cm^{-1} and show that $(H_2)InH_3$ [$(D_2)InD_3$] is a hypervalent complex involving three-center two-electron bonds. The HD counterpart for $(HD)InH_2D$ and $(HD)InHD_2$ absorbs at 3601.8 cm^{-1}. The

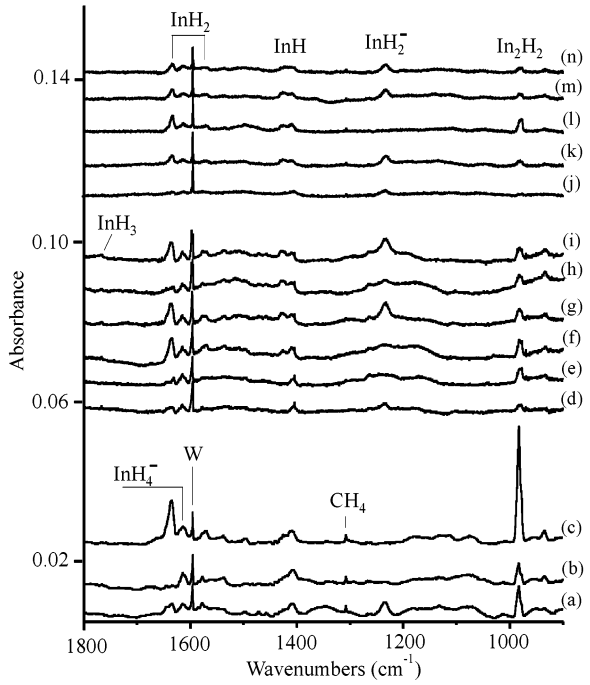

Figure 5. Infrared spectra in the 1800−900 cm^{-1} region for laser-ablated In codeposited with 4% H_2 in neon at 3.5 K in three experiments using different laser energies: (a) In deposited with 40 mJ/pulse, (b) after $\lambda > 380$ nm irradiation for 15 min, (c) after 240−380 nm irradiation, (d) In deposited with 20 mJ/pulse, (e) after $\lambda > 290$ nm irradiation, (f) after $\lambda > 240$ nm irradiation, (g) after 193 nm irradiation for 15 min, (h) after $\lambda > 530$ nm irradiation, (i) after 193 nm irradiation for 5 min, (j) In deposited with 10 mJ/pulse, (k) after 193 nm irradiation for 10 min, (l) after $\lambda > 240$ nm irradiation for 15 min, (m) after 193 nm irradiation for 10 min, and (n) after annealing to 8.0 K. W denotes water absorption.

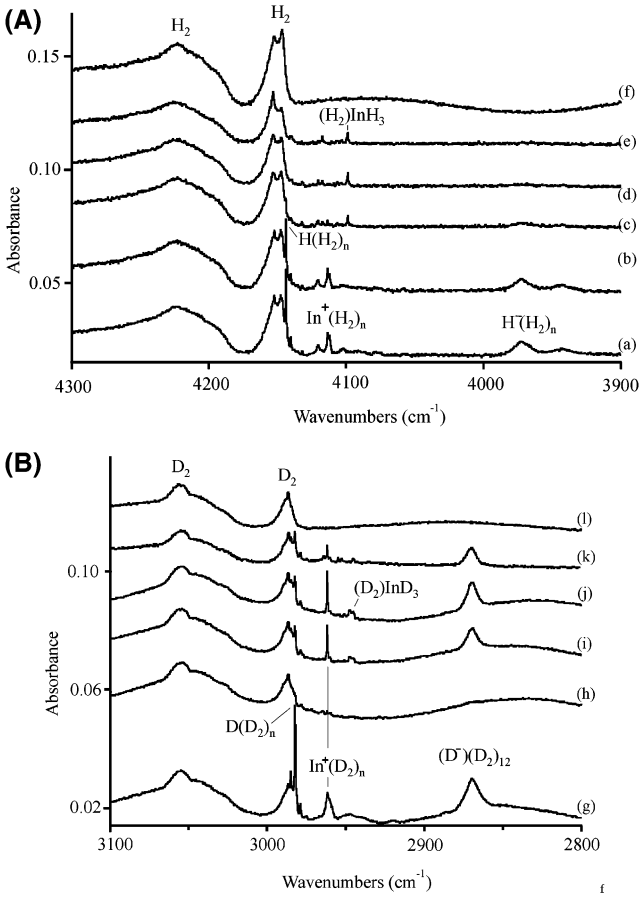

Figure 6. Infrared spectra in the 4300−3900 cm^{-1} region (A, top) and 3100−2800 cm^{-1} region (B, bottom) for laser-ablated In co-deposited with molecular hydrogen at 3.5 K: (a) spectrum of In + 3 mmol of H_2 deposited, (b) neon overcoat (1 mmol) deposited, (c) after 193 nm irradiation for 2 min at 4 mJ/pulse, (d) after 193 nm irradiation for 5 min, (e) after annealing to 6.5 K, (f) spectrum of pure H_2 (3 mmol) deposited, (g) spectrum of In + 3 mmol of D_2 deposited, (h) after $\lambda > 240$ nm irradiation for 15 min, (i) after 193 nm irradiation for 4 min, (j) after 193 nm irradiation for 8 min, (k) after annealing to 9.7 K, and (l) spectrum of pure D_2 (3 mmol) deposited and then irradiated at 193 nm for 8 min.

bonding interactions are progressively stronger with $(H_2)GaH_3$ absorption at 4087.3 cm^{-1} and $(H_2)(AlH_3)$ at 4061.6 cm^{-1} in the hypervalent complexes.[28,43] The sharp bands that appear on annealing at 1755.8 and 1739.2 cm^{-1} (deuterium counterparts at 1255.5 and 1245.9 cm^{-1}) are probably due to perturbed $(H_2)InH_3$ species. Figure 6 also shows two metal-independent absorptions at 4143.4 [2982.4] cm^{-1} and at 3972 [2870] cm^{-1} which have been assigned to H−H [D−D] vibrations in substitutional site complexes with H [D] and (H^-) [(D^-)], respectively.[28,43,44]

$In^+(H_2)_n$. A new metal-dependent absorption was observed at 4113.1 and 4111.7 [2961.8 and 2959.6] cm^{-1} in solid hydrogen [deuterium]. The HD counterpart is observed at 3595.3 cm^{-1}. These bands were destroyed by full mercury arc light and restored on 193 nm irradiation (a shifted 4117.3 cm^{-1} band appears). Figure 6 shows a slight decrease in the 4143.4, 4113.1, and 3972−3942 cm^{-1} bands on the application of a neon overcoat (1 mmol of neon over 3 mmol of H_2). Similar bands at 4108.9 and 4108.7 cm^{-1} with laser-ablated Ga and Al, respectively, have been assigned to $Ga^+(H_2)_n$ and $Al^+(H_2)_n$ complexes in solid hydrogen.[28,43] The 193 nm excitation exceeds the ionization energy of Ga and Al by 0.4 eV,[45] and the unusual blue shifts in this transition by the matrix[46,47] make ionization of these metals efficient. Since these $M^+(H_2)_n$ absorptions are regenerated by 193 nm irradiation, the same can be done for In. The radial extension of the indium atom is markedly increased by resonance transitions to 5d ($^2D_{3/2}$) and 6s ($^2S_{1/2}$) states, which causes large blue shifts in the atomic transitions. For the gas-phase 5p → 6s absorption at 410.3 nm, excitation in solid krypton is centered at 383 nm and emission followed at 428 and 477 nm.[48] As a result, strong broad In absorptions are observed at 6.4 eV in solid argon and neon,[49] and solid hydrogen and deuterium are expected to behave similarly. Hence, irradiation of In/H_2 and In/D_2 samples at 193 nm is expected to produce In^+ and e^-, and the regeneration of $In^+(H_2)_n$, $In^+(D_2)_n$, and $(D^-)(D_2)_{12}$ in Figure 6 follows: Unfortunately $(H^-)(H_2)_n$ is more photosensitive and cannot be so regenerated and trapped in the softer hydrogen matrix. Note also that In^+ cations are produced by laser ablation, and the trapping of In^+ in solid H_2 is a straightforward process.

Previous calculations have shown that the stable isomer for $Al^+(H_2)$ is the side-bound complex.[50,51] Although B3LYP calculations find an imaginary b_2 frequency, MP2 predicts a stable C_{2v} structure with a H−H fundamental red-shifted from the H_2 value by 46 cm^{-1}. However, what we have here is In^+ trapped in solid hydrogen interacting with a large number of (probably 12) H_2 ligands. This weak interaction is the reason for the small change from Al^+ to Ga^+ to In^+ complexes in solid hydrogen,[28,43] which may be represented as $M^+(H_2)_n$.

In_2H_2. Annealing the hydrogen and deuterium matrix samples increases weak bands at 979.6 and 709.9 cm^{-1} (H/D ratio 1.381). These bands are decreased by full arc irradiation and regenerated by further annealing. In contrast solid neon with 4% H_2 supports the marked growth of a strong 982.6 cm^{-1} band (Figure 5) with

TABLE 2: Calculated Structures and Vibrational Frequencies (cm^{-1}) (B3LYP/6-311++G(d,p)/LanL2DZ for Indium Hydrides

species	state	structure, Å, deg	rel energy (kcal/mol)	frequencies, cm^{-1} (symmetry, intensities, km/mol)
InH (C_v)	$^1\Sigma^+$	InH: 1.853		InH: 1406 (1005). InD: 999 (507)
InH_2 (C_{2v})	$^2A_1$	InH: 1.760	0.0	InH_2: 1636 (b_2, 534), 1597 (a_1, 126), 643 (a_1, 204)[a]
		HInH: 118.8		InD_2: 1164 (534), 1132 (65), 458 (103)
InH_2^- (C_{2v})	$^1A_1$	InH: 1.908	−27	InH_2^-: 1197 (a_1, 1915), 1176 (b_2, 1761), 692 (a_1, 208)[b]
		HInH: 91.5		InD_2^-: 850 (912), 836 (879), 492 (98)
$In^+(H_2)$ (C_{2v})	$^1A_1$	InH: 3.080	127	$In^+(H_2)$: 4369 (a_1, 59), 193 (a_1, 17), 129 i(b_2, 27)[c]
		HH: 0.747		
InH_2^+ (D_h)	$^1\Sigma_g$	InH: 1.668	157	InH_2^+: 1978 (σ_u, 7), 1888 (σ_g, 0), 594 (π_u, 93 × 2)
		HInH: 180.0		InD_2^+: 1411 (4), 1336 (0), 424 (51 × 2)
InH_3 (D_{3h})	$^1A_1$	InH: 1.728		InH_3: 1786 (a_1', 0), 1753 (e′, 346 × 2), 656 (e′, 245 × 2), 630 (a_2'', 347)
		HInH: 120		InD_3: 1264 (0), 1247 (180 × 2), 467 (124 × 2), 451 (178)
InH_4^- (T_d)	$^1A_1$	InH: 1.800		InH_4^-: 1591 (a_1, 0), 1479 (t_2, 832 × 3), 657 (e, 0 × 2), 656 (t_2, 644 × 3)[d]
				InD_4^-: 1125 (0), 1051 (426 × 3), 647 (0 × 2), 469 (317 × 3)
In_2H_2 (D_{2h})	^1A_g	InH: 2.059	0.0	In_2H_2: 1149 (a_g, 0), 1039 (b_{1u}, 2370), 852 (b_{3g}, 0), 802 (b_{2u}, 328), 341 (b_{3u}, 9), 137 (a_g, 0)
		InHIn: 110.9		In_2D_2: 813 (0), 738 (1196), 604 (0), 570 (166), 242 (4), 137 (0)
In_2H_2 (C_{2v})	$^1A_1$	InIn: 3.117	14	$InInH_2$: 1617 (a_1, 761), 1608 (b_2, 519), 662 (a_1, 544), 307 (b_1, 126), 177 (b_2, 36), 118 (a_1, 6)
		InH: 1.768		InInHD: 1612 (655), 1146 (308), 1146 (308), 576 (412), 267 (95), 145 (24), 117 (6)
		HInH: 110.0		$InInD_2$: 1147 (385), 1144 (263), 471 (270), 220 (64), 127 (18), 117 (6)
In_2H_2 (C_{2h})	^1A_g	InH: 1.804	17	HInInH: 1517 (b_u, 1612), 1506 (a_g, 0), 404 (a_g, 0), 163 (a_u, 34), 153 (b_u, 25), 87 (a_g, 0)
		InIn: 3.088		
		InInH: 119.3		
In_2H_4 (C_{2v})	$^1A_1$	InH: 1.727	0.0	$In(H)_2InH_2$: 1763 (a_1, 148), 1748 (b_2, 332), 1397 (a_1, 622), 1140 (b_1, 3), 1013 (a_1, 1159), 885 (b_1, 561), 703 (b_2, 207), 609 (a_1, 464), 585 (a_2, 0), 408 (b_1, 15), 156 (b_2, 8), 145 (a_1, 6)
		$In(H)_2In$: 1.899, 2.109		
		HInH: 125.9		
		InH_2: 79.9, 70.7		
In_2H_4 (C_{3v})	$^1A_1$	$In(H)_3In$: 2.291, 1.845	2	$In(H)_3InH$: 1809 (a_1, 360), 1540 (a_1, 219), 1371 (e, 104 × 2), 758 (e, 126 × 2), 738 (a_1, 1105), 666 (e, 294 × 2), 211 (e, 13 × 2), 169 (a_1, 18)
		InH: 1.707		
		HInH: 66.9, 86.4		
		HInH: 127.7		
In_2H_4 (D_{2d})	$^1A_1$	InH: 1.740	11	In_2H_4: 1729 (a_1, 0), 1704 (b_2, 629), 1703 (e, 393 × 2), 689 (a_1, 0), 619 (b_2, 806), 462 (e,73 × 2), 153 (a_1, 0), 145 (b_1, 0)
		HInH: 115.9		
		InIn: 2.844		
In_2H_6 (D_{2h})	^1A_g	InH: 1.940		In_2H_6: 1818 (a_g, 0), 1814 (b_{3u}, 129), 1810 (b_{2u}, 558), 1803 (b_{1g}, 0), 1351 (a_g, 0), 1280 (b_{3u}, 1372), 1165 (b_{2g}, 0), 1062 (b_{1u}, 486), 751 (b_{2u}, 307), 669 (b_{3g}, 0), 629 (a_g, 0), 574 (b_{3u}, 784), 567 (b_{1u}, 239), 387 (b_{1g}, 0), 364 (a_u, 0), 345 (b_{2g}, 0), 205 (b_{2u}, 7), 161 (a_g, 0)
		InH: 1.712		
		InHIn: 100.8		
		HInH: 131.1		

[a] MP2 calculation gives 1.737 Å, 118.8°, 1722 cm^{-1} (b_2, 599 km/mol), 1711 cm^{-1} (a_1, 180 km/mol), and 669 cm^{-1} (a_1, 231 km/mol). [b] MP2 calculation gives 1.885 Å, 91.4°, 16 kcal/mol energy below InH_2, 1254 cm^{-1} (a_1, 1808 km/mol), 1216 cm^{-1} (b_2, 1773 km/mol), and 745 cm^{-1} (a_1, 329 km/mol). [c] MP2 calculation gives 3.180 Å, 0.740 Å, 4469 cm^{-1} (a_1, 44 km/mol), 237 cm^{-1} (b_2, 9 km/mol), and 194 cm^{-1} (a_1, 12 km/mol). [d] MP2 calculation gives 1.790 Å, 1618 cm^{-1} (a_1, 0), 1504 cm^{-1} (t_2, 817 × 3 km/mol), 677 cm^{-1} (t_2, 656 × 3 km/mol), and 671 cm^{-1} (e, 0 × 2 km/mol).

a D_2 counterpart at 711.7 cm^{-1} (H/D ratio 1.380). These absorptions are higher than recently observed 954.8 and 693.1 cm^{-1} absorptions for In_2H_2 in solid argon,[42] but the shifts are reasonable for assignment to rhombic In_2H_2.[52] The larger argon−hydrogen−neon matrix shift observed for In_2H_2 relative to InH_{1-3} species demonstrates a greater matrix interaction for the bridged In(μ-H)$_2$In bonds. In neon with 5% HD a strong 923.2 cm^{-1} feature is produced on irradiation, which is appropriate for the lower symmetry In_2HD molecule. The 923.2 cm^{-1} band decreases on annealing as do InH and InD absorptions, while broad 979 and 700 cm^{-1} bands appear: The latter are due to In_2H_2 and In_2D_2, respectively, produced by a different mechanism.

Himmel et al.[42] suggest that In_2H_2 is formed by near-UV photolysis of In_2 with H_2 in solid argon, and our solid neon observations are in agreement. In addition annealing appears to allow dimerization of InH to form In_2H_2, but the latter reaction is not as efficient.

$$In_2 + H_2 \xrightarrow{UV} In_2H_2 \quad (1)$$

$$InH + InH \rightarrow In_2H_2 \quad (2)$$

Weak bands at 1529.9 cm^{-1} in solid H_2 and at 1102.9 cm^{-1} in solid D_2 (H/D ratio 1.387) are due to another diindium dihydride species. Neon matrix counterparts are found at 1537.3 and 1104.6 cm^{-1} (H/D ratio 1.392). The lower intermediate bands with HD at 1528.7 and 1101.3 cm^{-1} strongly suggest assignment to the $InInH_2$ isomer rather than to HInInH as proposed by Himmel et al. for the 1518 cm^{-1} argon matrix band without HD isotopic observations. In addition the second strongest band, a bending mode, is observed at 628.7 cm^{-1} with a D_2 counterpart at 456.0 cm^{-1} (H/D ratio 1.379). Our B3LYP calculations and earlier B3PW91 calculations[42] show that the two terminal stretching modes are very close, so the observed split band is probably due to both stretching modes. Furthermore, the $InInH_2$ isomer is computed to be 4 kcal/mol more stable than HInInH.

In_2H_4. New photosensitive absorptions can be assigned to In_2H_4 isomers but with less confidence owing to the low yields. Recall that Al_2H_4 and Ga_2H_4 were observed in analogous experiments.[24,25,28,43] Following the latter examples,[53,54] three In_2H_4 isomers are stable, $C_{2v} < C_{3v} < D_{2d}$, as shown by the B3LYP calculations given in Table 2. The $In(H)_2InH_2$ structure is predicted to have very strong absorptions at 1013 and 885 cm^{-1}, and we have no absorptions in this region other than In_2H_2 at 979.6 cm^{-1}. The $In(H)_3InH$ isomer is computed to be only 2.4 kcal/mol higher in energy, and its strongest absorption, the a_1 bridge−H stretching mode, is computed at 738 cm^{-1} with

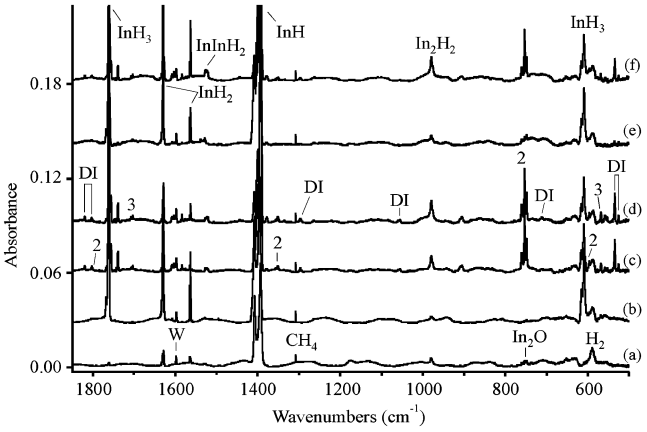

Figure 7. Infrared spectra in the 1850−500 cm^{-1} region for laser-ablated In codeposited with pure normal isotopic hydrogen samples at 3.5 K: (a) pure H_2 and In deposited, (b) after 193 nm irradiation for 15 min, (c) after annealing to 6.2 K, (d) after annealing to 7.2 K, (e) after 193 nm irradiation for 4 min, and (f) after annealing to 7.0 K.

TABLE 3: Comparison of the Strongest Calculated and Observed Frequencies (cm^{-1}) for Diindane (4) In_2H_4 Isomers

$In(H)_2InH_2$ (C_{2v})	$In(H)_3InH$ (C_{3v})	In_2H_4 (D_{2d})
1763	1809 (1802.0)[b]	1704 (1707.0)
1748	1540, n.o.	1702[a] (1703.6)
1397,[a] n.o.	1371 (1351.3)	619[a] (568.2)
1013,[a] n.o.	758 (760.1)	462, n.o.
886,[a] n.o.	738 (753.8)	
702	666 (597.5)	
609		

[a] Strongest calculated modes: See Table 2. n.o. = not observed. [b] Observed values in parentheses.

the e counterpart at 758 cm^{-1}. Three sharp bands at 760.2, 753.3, and 748.1 cm^{-1} are destroyed by UV irradiation and regenerated by further annealing. The weaker 760.2 cm^{-1} band is probably due to the e mode, and the two stronger 753.3 and 748.1 cm^{-1} bands are probably due to the stronger a_1 mode. Associated bands for this species appear at 1802.0, 1351.2, and 597.5 cm^{-1} and are labeled 2 in Figure 7. The weak, broad band at 907 cm^{-1} that appears on annealing cannot be identified without more information. Unfortunately, our $H_2 + D_2$ and HD spectra are too complicated to assist with the identification of In_2H_4. Table 3 summarizes these assignments. The analogous Al species was observed at 924 and 844 cm^{-1}.[25]

The InH_2InH_2 (D_{2d}) structure is another 11 kcal/mol higher in energy, but three bands are observed at 1707.0, 1703.6, and 568.2 cm^{-1} for this molecule (labeled 3 in Figure 7). The analogous species have been observed for Al and Ga at higher frequencies, 1875, 1863, and 730 cm^{-1} and 1838, 1826, and 747 cm^{-1}, respectively.[25,28]

In_2H_6. We also find very good evidence for dibridged In_2H_6 molecules: This dimer is produced during the later stages of annealing solid hydrogen at 6−8 K at the apparent expense of InH_3, which suggests a very small barrier to dimerization. Although In_2H_2 also increases on annealing, reaction 2, the further addition of $2H_2$ to form In_2H_6 probably requires substantial activation energy. The dimerization reaction 3

$$2InH_3 \rightarrow In_2H_6 \quad (3)$$

$$nInH_3 \rightarrow (InH_3)_n \quad (4)$$

is the most likely mechanism for the formation of In_2H_6, a product not formed in solid neon where the concentrations of InH and In_2H_2 are high but the yield of InH_3 is low. Reaction 3 is calculated to be exothermic by 1 kcal/mol,[7] which is in contrast to the much more exothermic alane reaction to dialane.[24,25] Furthermore, In_2H_6 is predicted from earlier calculations to be a stable molecule at low temperature.[7] Unfortunately, In_2H_6 decomposes on $\lambda > 240$ nm photolysis, so its yield is limited compared to that of the more stable Al_2H_6 molecule.[25,43] The new 1820.0, 1803.4, 1297.0, 1059.0, 717.9, 534.6, and 525.5 cm^{-1} absorptions (labeled DI for diindane) that appear on late annealing after UV irradiation are appropriate for dibridged In_2H_6 on the basis of comparisons with recent MP2 calculations,[7] our B3LYP frequencies (Table 4), and the spectrum of Al_2H_6 in solid hydrogen.[25] The two terminal In−H_2 modes at 1820.0 and 1803.4 cm^{-1} are higher than for InH_3, as calculated and observed, and as found for the aluminum analogues. The two In−H−In bridging modes at 1297.0 and 1059.0 cm^{-1} are 17 cm^{-1} above and 3 cm^{-1} below our B3LYP calculated values, and of course below the observed values for Al_2H_6. The 1297.0 cm^{-1} absorption may suffer perturbation by the hydrogen matrix. The three lower frequency bands are 33−41 cm^{-1} below calculated values as expected. Our In_2H_6 identification rests on very good agreement between seven observed and calculated fundamentals.

TABLE 4: Comparison of Calculated and Observed Frequencies (cm^{-1}) for Diindane (6) In_2H_6

MP2[a]	B3LYP[b]	obsd[c]	obsd[d]	H/D ratio
1841	1814 (b_{3u}, 129)	1820 (0.004)	1297	1.403
1837	1810 (b_{2u}, 558)	1803 (0.002)	1291	1.397
1262	1280 (b_{3u}, 1372)	1297 (0.011)	943	1.375
1089	1062 (b_{1u}, 486)	1059 (0.005)	767	1.381
753	751 (b_{2u}, 307)	718 (0.005)		
607	574 (b_{3u}, 784)	535 (0.034)		
588	567 (b_u, 239)	526 (0.008)		

[a] Reference 7. [b] This work (mode symmetry and intensity, km/mol). [c] This work in solid hydrogen (integrated absorbances). [d] This work in solid deuterium.

Solid Indane $(InH_3)_n$. The spectrum after removal of the H_2 matrix sample shows that the sharp product absorptions are replaced by a broad (300 cm^{-1} full width at half-maximum) band centered at 1460 ± 20 cm^{-1} (Figure 1f). Similar behavior was observed for In in D_2: The strong InD band at 997.7 cm^{-1} is replaced by InD_3 at 1266.2 cm^{-1} (Figure 2b,c), and annealing replaces these sharp absorptions with a broad (200 cm^{-1} full width at half-maximum) band centered at 1060 ± 20 cm^{-1} (Figure 2f). Spectra were recorded for both samples continuously as they warmed to room temperature without operating the cryogenic refrigerator. The broad 1460 cm^{-1} band in H_2 experiments is observed in spectra recorded at 40−50 K, and in sets of spectra recorded from 60 to 160 K, but it is decreased in the 160−180 K spectrum (not shown) and absent from the spectrum recorded at 180−200 K (Figure 1g). The broad 1060 cm^{-1} band in spectra with D_2 at 30−60 K (Figure 2e) remains in the spectra recorded until the window reaches 200−220 K (Figure 2g). Indium metal is left on the window at room temperature, but solid $(AlH_3)_n$ and not aluminum metal was found in the analogous Al experiments where about half of the alane film absorption remains on the window at 290 K.[24,25]

Infrared spectra for Al, Ga, and In experiments with pure hydrogen are compared in Figure 9. The Al spectrum shows the seven Al_2H_6 fundamentals (DA) and the strong AlH_3 bands after annealing and 193 nm irradiation (Figure 9a). Annealing to 7 K allows the H_2 matrix to evaporate, and the spectrum recorded at 100−120 K (Figure 9b) illustrates the broad 1720

and 720 cm^{-1} $(AlH_3)_n$ bands.[25] Similar experiments with laser-ablated Ga in pure H_2 give GaH, GaH_2, and GaH_3 absorptions, and 193 nm irradiation and annealing produced weak Ga_2H_6 absorptions.[28] After the H_2 matrix evaporated, broad absorptions at 1800−2000, 1300−1700, and 600−700 cm^{-1} (Figure 9) remained until the window reached 260 K: At room temperature the window is free of gallane. Our broad bands are similar to features in the spectrum of solid gallane oligomers containing both terminal and bridged Ga−H bonds, which evaporate digallane on warming to 210 K.[30] Spectra from another In experiment using higher laser energy are shown in Figure 9 after 193 nm irradiation and after warming to 60−80 K, respectively. The broad 1460 cm^{-1} band replaces the sharp indium hydride absorptions on annealing. Although the solid indane film formed contains lower oxidation state indium hydrides, the broad 1460 cm^{-1} band is dominated by indium(III) hydride, and it is certainly the best model for solid indane observed to date. Note that the yield of AlH_3 exceeds the yields of GaH_3 and InH_3 in these hydrogen matrix experiments.[24,25,28,43]

The present observation of solid indane, which decomposes at 180−190 K, shows that the earlier claim for a room temperature stable indane solid[1,2] is not correct. Our observation is in agreement with theoretical predictions of limited stability for solid indane.[7]

The chemistry of Al, Ga, and In is influenced by a d-orbital contraction for Ga, which reduces the atomic size and makes Ga more electronegative. Thus, Al is more electropositive, a better Lewis acid, and stabilizes the 6-fold coordination network with Al−H−Al bridge bonds in solid $(AlH_3)_n$.[27] In contrast solid gallane has an oligomer structure with both terminal and bridging Ga−H bonds.[30] Shell expansion leads to a larger atomic radius for In, which is more electropositive than Ga, and In will therefore favor the 6-fold coordination with In−H−In bridge bonds in solid $(InH_3)_n$ similar to $(AlH_3)_n$.

Other Absorptions. A new absorption observed at 1234 cm^{-1} in neon/H_2 samples codeposited with laser-ablated In shifted to 893 cm^{-1} with neon/D_2 (H/D ratio 1.382). These bands are destroyed by visible light (decreased by $\lambda > 530$ nm, almost destroyed by $\lambda > 470$ nm, destroyed by $\lambda > 380$ nm). However, irradiation at 193 nm, which is capable of ionizing In, produces an even stronger 1534 cm^{-1} absorption (Figure 5g). After reduction by visible light, InH_2 at 1636 cm^{-1} and the 1234 cm^{-1} absorption are regenerated by 193 nm irradiation (Figure 5i). Note that 240−380 nm irradiation produces InH_2 but not the 1234 cm^{-1} band (Figure 5c). Similar experiments with neon/HD gave slightly different broad absorptions at 1237 and 893 cm^{-1}. Solid molecular hydrogens produced a lower yield of this species. A weak H_2 counterpart was observed at 1225 cm^{-1} with D_2 product at 883 cm^{-1} (H/D ratio 1.386) (Figure 8).

The observation of GaH_2^- at 1350 cm^{-1} in solid neon suggests a tentative assignment of the analogous 1234 cm^{-1} indium product as InH_2^-. The strongest mode of InH_2 is 8.6% below the analogous mode for GaH_2, and the 1234 cm^{-1} band is also 8.6% below the 1350 cm^{-1} GaH_2^- fundamental. Although B3LYP/LANL2DZ/6-311++G(d,p) calculations predict InH_{1-3} stretching frequencies within 2%, frequencies for the stable, bent InH_2^- anion are predicted 3−5% low. However, MP2 calculations[35] in Gaussian 98 predict higher frequencies at 1254 and 1216 cm^{-1}, which bracket the observed value. The problem here is that LANL2DZ calculations predict two modes separated more than our bandwidth, and if these calculations are correct, the 1234 cm^{-1} absorption will have to be reassigned to another transient indium hydride species. We expect that the

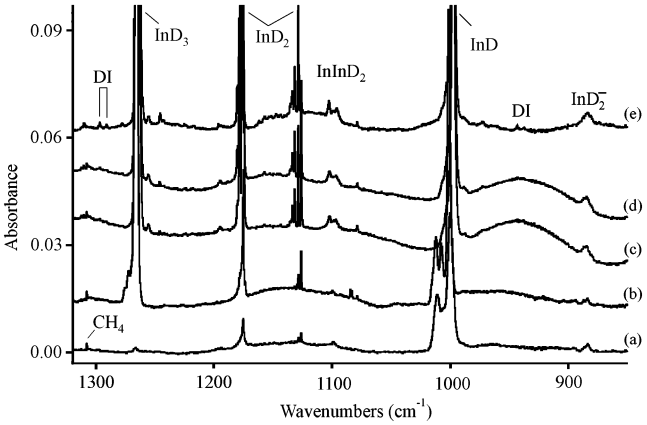

Figure 8. Infrared spectra in the 1300−850 cm^{-1} region for laser-ablated In codeposited with pure D_2 at 3.5 K: (a) D_2 and In deposited, (b) after 193 nm irradiation for 20 min, (c) after annealing to 10.0 K, (d) after annealing to 10.5 K, and (e) after annealing to 11.6 K.

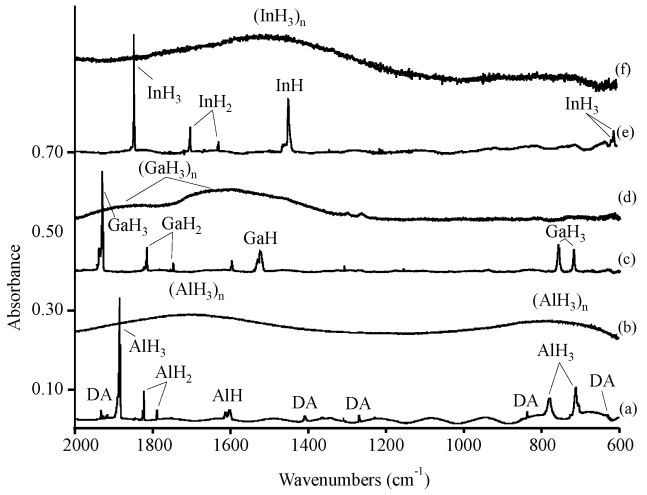

Figure 9. Infrared spectra of samples prepared by codepositing laser-ablated group 13 metal atoms with pure normal hydrogen at 3.5 K: (a) Al after deposition and 193 nm irradiation for 20 min (DA identifies dialane, Al_2H_6), (b) after warming to 100−120 K, (c) Ga after deposition and 193 nm irradiation for 12 min, (d) after warming to 110−130 K, (e) In after 193 nm irradiation for 30 min, and (f) after warming to 60−80 K.

1234 cm^{-1} observed band is due to both InH_2^- stretching modes not resolved. In any case the LANL2DZ basis set is too small, and higher level calculations will be required for a better calculation of this heavy metal dihydride anion.

Our neon matrix experiments also revealed a 1613 cm^{-1} band that increased slightly on $\lambda > 380$ nm irradiation with the disappearance of InH_2^- and decreased slightly on irradiation at 240−380 nm (Figure 4b). A weak neon/D_2 counterpart is observed at 1161 cm^{-1} (H/D ratio 1.389). Weak H_2 [D_2] matrix counterparts are found at 1608 [1152] cm^{-1}. Unfortunately InHD falls in both regions, so no mixed isotopic data are available. On the basis of agreement with the 1640−1600 cm^{-1} absorption reported for alkali-metal−InH_4^- salts,[8] we tentatively assign the 1613 cm^{-1} band to the antisymmetric stretching fundamental of isolated InH_4^-. We note that $LiInH_4$ is employed as a synthetic precursor.[11] Although our B3LYP calculation predicts this fundamental at 1479 cm^{-1}, which is too low because of the inadequate basis set for In, the MP2 method gives a higher value, 1504 cm^{-1}, for the strong mode of tetrahedral InH_4^-. Clearly, higher level calculations are needed. We note that Lewis

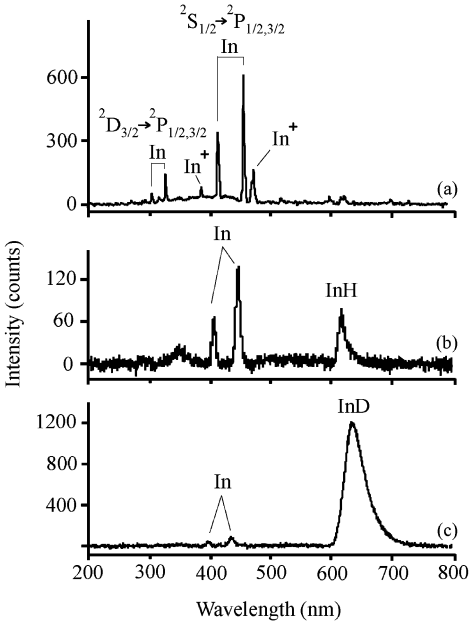

Figure 10. Emission spectra from laser-ablated indium experiments: (a) spectrum from the plume above the indium target excited by pulsed, focused 1064 nm excitation, (b) spectrum from solid H_2 codeposited with laser-ablated In using 193 nm excitation, (c) spectrum from solid D_2 codeposited with laser-ablated In using 193 nm excitation.

acid−base reaction 6 is highly exothermic.

$$InH_2^- + H_2 \xrightarrow{\lambda > 380\ nm} InH_4^- \ (\Delta E = -27\ kcal/mol) \quad (5)$$

$$InH_3 + H^- \rightarrow InH_4^- \ (\Delta E = -67\ kcal/mol) \quad (6)$$

Emission Spectra. Complementary emission spectra were recorded to support this infrared absorption study of indium hydrides. The strong purple emission in the laser ablation plume from the target surface was dominated by the strong spin−orbit split indium $^2S_{1/2} \rightarrow {}^2P_{1/2,\ 3/2}$ doublet at 410.3 and 451.3 nm, which was used to calibrate the spectrometer.[45] The weaker indium $^2D_{3/2} \rightarrow {}^2P_{1/2,\ 3/2}$ doublet at 303.9 and 325.6 nm and In^+ lines at 383.5 and 468.5 nm were observed (Figure 10).[45,55] The In^+ emission intensities were particularly sensitive to laser energy, and In^+ complexes with hydrogen can be formed directly in these experiments.

Irradiation at 193 nm of In and InD in solid deuterium, such as that contained in the sample whose infrared spectrum is shown in Figure 2a, produced a strong red emission visible to the naked eye. This red emission peaked at 636 ± 1 nm, and weaker sharp lines were observed at 398.1 and 436.2 ± 0.3 nm. Similar treatment of In and InH in solid hydrogen, such as that responsible for the infrared spectrum shown in Figure 1a, gave a weak purple emission to the eye. The emission spectrum reveals a sharp red 615.0 ± 0.3 nm emission, and sharp 405.2 and 444.8 ± 0.3 nm lines. The absolute emission intensities of the sharp doublets are about the same in the two solid molecular hydrogens (Figure 10).

The sharp doublets are due to the $^2S_{1/2} \rightarrow {}^2P_{1/2,3/2}$ emission of In observed in the gas phase at 410.3 and 451.3 nm.[45] The doublets are blue-shifted 320 ± 20 cm^{-1} in solid hydrogen and 760 ± 20 cm^{-1} in solid deuterium. The spin−orbit splitting observed for In in solid H_2 and D_2 (2200 ± 20 cm^{-1}) matches the gas-phase value (2213 cm^{-1}) within experimental error. Such emissions are red-shifted about 1000 cm^{-1} in solid krypton.[48] The greater blue shift in solid D_2 than in solid H_2 is attributed to enhanced repulsion due to the smaller lattice constant for solid D_2 (3.600 Å) compared to H_2 (3.769 Å).[56,57]

The red emissions are assigned to the a $^3\Pi(0^+) \rightarrow X^1\Sigma^+$ phosphorescence of InH [InD] in solid hydrogen [deuterium] on the basis of near agreement with the gas-phase 614.3 nm band origin.[13] We note that the red emission is much weaker in solid H_2 than in solid D_2, and we suggest that the nonradiative relaxation rate in solid H_2 is much faster due to the larger zero-point vibrational amplitude in solid H_2.[58]

Similar irradiation of solid neon samples containing laser-ablated In gave sharp 455.0 nm and weaker 413.5 nm emissions for In and broad 420, 392, 367, 343, and 320 nm emissions for In_x species. Solid neon containing H_2 gave the same broad bands plus a 616.4 nm feature, which is probably due to InH.

Conclusions

Laser-ablated In atoms react with H_2 to form InH, which is efficiently converted to InH_3 on 193 nm irradiation. Visible radiation destroys InH_2, but near-ultraviolet light initiates the insertion reaction to form InH_2. Although In_2H_2 is formed mostly from the photoreaction of In_2 and H_2, In_2H_4 and In_2H_6 appear to arise from dimerization processes during 6−8 K annealing. A neon overcoat extended the annealing range of solid H_2 by 0.5 K and made possible the diffusion and dimerization of InH_3 to form In_2H_6 for the first time. Upon evaporation of the solid H_2 matrix, a solid indane film forms and remains until the substrate reaches 180−190 K. Charged species are also observed in these experiments: The In^+ cation forms a weak dihydrogen complex analogous to Ga^+ and Al^+ in solid hydrogen. From Al to Ga to In we find decreasing abundance of MH_4^-, increasing stability of MH_2^-, and decreasing stability of the dibridged M_2H_6 molecules and the $(MH_3)_n$ solids. Similar hydrogen experiments with Tl give absorptions for the analogous TlH and TlH_2 species, a low yield of TlH_3, and no evidence for the solid $(TlH_3)_n$.[59] A very recent review article casts strong doubt on the original claim for the preparation of room temperature stable solid indane and thallane.[60] Our TlH_3 band absorbance is much less than observed for InH_3, which in turn is much less than observed for GaH_3 and AlH_3, and is the expected vertical periodic trend.[7]

In this work, and in similar experiments with alane,[24,25] we demonstrate a new synthetic method for pure metal hydrides of limited stability, and use this to form solid indane, which decomposes at 180−190 K. The metal hydride intermediates formed by reactions of metal atoms with hydrogen and isolated in solid hydrogen are allowed to react at 7 K on evaporation of the hydrogen matrix, and the pure metal hydride reaction product film can be monitored by infrared spectroscopy up to room temperature.

Acknowledgment. We gratefully acknowledge support for this work from NSF Grant CHE 00-78836 and helpful discussions with P. Schwerdtfeger.

References and Notes

(1) Wiberg, E.; Schmidt, M. *Z. Naturforsch., B* **1952**, *7*, 577.
(2) Wiberg, E.; Dittmann, O. *Z. Naturforsch., B* **1957**, *12*, 57.
(3) Breisacher, P.; Siegel, B. *J. Am. Chem. Soc.* **1965**, *87*, 4255.
(4) Taylor, M. J.; Brothers, P. J. In *Chemistry of Aluminum Gallium, Indium, and Thallium*; Downs, A. J., Ed.; Blackie: Glasgow, Scotland, 1993; p 111.
(5) Downs, A. J.; Pulham, C. R. *Chem. Soc. Rev.* **1994**, *1994*, 175.
(6) Aldridge, S.; Downs, A. J. *Chem. Rev.* **2001**, *101*, 3305.
(7) Hunt, P.; Schwerdtfeger, P. *Inorg. Chem.* **1996**, *35*, 2085.
(8) Bakum, S. I.; Kuznetsova, S. F.; Tarasov, V. P. *Zh. Neorg. Khim.* **1999**, *44*, 346.

(9) Hibbs, D. E.; Hursthouse, M. B.; Jones, C.; Smithies, N. A. *Chem. Commun.* **1998**, 869.
(10) Abernethy, C. D.; Cole, M. L.; Jones, C. *Organomet.* **2000**, *19*, 4852.
(11) Jones, C. *J. Chem. Soc., Chem. Commun.* **2001**, 2293 and references therein.
(12) Neuhaus, H. *Z. Phys.* **1958**, *152*, 402.
(13) Ginter, M. L. *J. Mol. Spectrosc.* **1963**, *11*, 301.
(14) Ginter, M. L. *J. Mol. Spectrosc.* **1966**, *20*, 240.
(15) Huber, K. P.; Herzberg, G. *Constants of Diatomic Molecules*; Van Nostrand: Princeton, NJ, 1979.
(16) Bahnmaier, A. H.; Urban. R. D.; Jones, H. *Chem. Phys. Lett.* **1989**, *155*, 269.
(17) White, J. B.; Dulick, M.; Bernath, P. F. *J. Mol. Spectrosc.* **1995**, *169*, 410.
(18) Ito, F.; Nakanaga, T.; Tako, H. *J. Mol. Spectrosc.* **1995**, *169*, 421.
(19) Pullumbi, P.; Mijoule, C.; Manceron, L.; Bouteiller, Y. *Chem. Phys.* **1994**, *185*, 13.
(20) Pullumbi, P.; Bouteiller, Y.; Manceron, L.; Mijoule, C. *Chem. Phys.* **1994**, *185*, 25.
(21) Balasubramanian, K.; Tao, J. X. *J. Chem. Phys.* **1991**, *94*, 3000.
(22) Bauschlicher, C. W., Jr. *J. Phys. Chem. A* **1999**, *103*, 6429.
(23) Cardelino, B. H.; Moore, C. E.; Cardelino, C. A.; Frazier, D. O. *J. Phys. Chem. A* **2001**, *105*, 849.
(24) Andrews, L.; Wang, X. *Science* **2003**, *299*, 2049.
(25) Wang, X.; Andrews; L.; Tam, S.; DeRose, M. E.; Fajardo, M. E. *J. Am. Chem. Soc.* **2003**, *125*, 9218.
(26) Matzek, W. E.; Musinski, D. F. U.S. Patent 3,883,644, 1975; *Chem. Abstr.* **1975**, *83*, 45418.
(27) Turley, J. W.; Rinn, H. W. *Inorg. Chem.* **1969**, *8*, 18.
(28) Wang, X.; Andrews, L. *J. Phys. Chem. A* **2003**, *107*, 11371 (Ga + H_2).
(29) Downs, A. J.; Goode, M. J.; Pulham, C. R. *J. Am. Chem. Soc.* **1989**, *111*, 1936.
(30) Pulham, C. R.; Downs, A. J.; Goode, M. J.; Rankin, D. W. H.; Robertson, H. E. *J. Am. Chem. Soc.* **1991**, *113*, 5149.
(31) Andrews, L.; Wang, X. *Angew. Chem., Int. Ed.* **2004**, *43*, 1706.
(32) (a) Andrews, L.; Citra, A. *Chem. Rev.* **2002**, *102*, 885. (b) Wang, X.; Andrews, L. *J. Phys. Chem. A* **2003**, *107*, 570. (c) Andrews, L. *Chem. Soc. Rev.* **2004**, *33*, 123.
(33) Wang, X.; Andrews, L.; Chertihin, G. V.; Souter, P. F. *J. Phys. Chem. A* **2002**, *106*, 6302.
(34) Andrews, L.; Wang, X.; Manceron, L. *J. Chem. Phys.* **2001**, *114*, 1559.
(35) Frisch, M. J.; Trucks, G. W.; Schlegel, H. B.; Scuseria, G. E.; Robb, M. A.; Cheeseman, J. R.; Zakrzewski, V. G.; Montgomery, J. A., Jr.; Stratmann, R. E.; Burant, J. C.; Dapprich, S.; Millam, J. M.; Daniels, A. D.; Kudin, K. N.; Strain, M. C.; Farkas, O.; Tomasi, J.; Barone, V.; Cossi, M.; Cammi, R.; Mennucci, B.; Pomelli, C.; Adamo, C.; Clifford, S.; Ochterski, J.; Petersson, G. A.; Ayala, P. Y.; Cui, Q.; Morokuma, K.; Malick, D. K.; Rabuck, A. D.; Raghavachari, K.; Foresman, J. B.; Cioslowski, J.; Ortiz, J. V.; Stefanov, B. B.; Liu, G.; Liashenko, A.; Piskorz, P.; Komaromi, I.; Gomperts, R.; Martin, R. L.; Fox, D. J.; Keith, T.; Al-Laham, M. A.; Peng, C. Y.; Nanayakkara, A.; Gonzalez, C.; Challacombe, M.; Gill, P. M. W.; Johnson, B. G.; Chen, W.; Wong, M. W.; Andres, J. L.; Head-Gordon, M.; Replogle, E. S.; Pople, J. A. *Gaussian 98*, revision A.7; Gaussian, Inc.: Pittsburgh, PA, 1998.
(36) (a) Becke, A. D. *J. Chem. Phys.* **1993**, *98*, 5648. (b) Stevens, P. J.; Devlin, F. J.; Chablowski, C. F.; Frisch, M. J. *J. Phys. Chem.* **1994**, *98*, 11623.
(37) (a) Krishnan, R.; Binkley, J. S.; Seeger, R.; Pople, J. A. *J. Chem. Phys.* **1980**, *72*, 650. (b) Frisch, M. J.; Pople, J. A.; Binkley, J. S. *J. Chem. Phys.* **1984**, *80*, 3265.
(38) Wadt, W. R.; Hay, P. J. *J. Chem. Phys.* **1985**, *82*, 284.
(39) (a) Becke, A. D. *Phys. Rev. A* **1988**, *38*, 3098. (b) Perdew J. P. *Phys. Rev. B* **1983**, *33*, 8822. (c) Perdew, J. P.; Wang, Y. *Phys. Rev. B* **1992**, *45*, 13244.
(40) Burkholder, T. R.; Yustein, J. T.; Andrews, L. *J. Phys. Chem.* **1992**, *96*, 10089.
(41) Hauge, R. H.; Kauffman, J. W.; Margrave, J. L. *J. Am. Chem. Soc.* **1980**, *102*, 6005.
(42) Himmel, H.-J.; Manceron, L.; Downs, A. J.; Pullumbi, P. *J. Am. Chem. Soc.* **2002**, *124*, 4448.
(43) Wang, X.; Andrews, L. *J. Phys. Chem. A*, **2004**, *108*, 4202−5320.
(44) Wang, X.; Andrews, L. *J. Phys. Chem. A* **2004**, *108*, 1103.
(45) Moore, C. E. *Atomic Energy Levels*; Circular 467; National Bureau of Standards: Washington, DC, 1952.
(46) Ammeter J. H.; Schlosnagle, D. C. *J. Chem. Phys.* **1973**, *59*, 4784.
(47) Abe, H.; Kolb, D. M. *Ber. Bunsen-Ges. Phys. Chem.* **1983**, *87*, 523.
(48) Balling, L. C.; Wright, J. J. *J. Chem. Phys.* **1981**, *74*, 6554.
(49) Schroeder, W.; Rotermund, H.-H.; Wiggenhauser, H.; Schrittenlacher, W.; Hormes, J.; Krebs, W.; Laaser, W. *Chem. Phys.* **1986**, *104*, 435.
(50) Niu, J.; Rao, B. K.; Jena, P. *Phys. Rev. B* **1995**, *51*, 4475.
(51) Rasul, G.; Prakash, G. K. S.; Olah, G. A. *J. Phys. Chem. A* **2000**, *104*, 2284.
(52) Treboux, G.; Barthelat, J.-C. *J. Am. Chem. Soc.* **1993**, *115*, 4870.
(53) Lammertsma, K.; Güner, O. F.; Drewes, R. M., Reed, A. E.; Schleyer, P. v. R. *Inorg. Chem.* **1989**, *28*, 313.
(54) Lammertsma, K.; Leszczynski, J. *Inorg. Chem.* **1990**, *94*, 5543.
(55) Line Spectra of the Elements. *CRC Handbook*, 66th ed.; CRC Press: Boca Raton, FL, 1985.
(56) Krupskii, I. N.; Prokhvatilov, A. I.; Shcherbakov, G. N. *Sov. J. Low Temp. Phys.* **1983**, *9*, 446.
(57) Shcherbakov, G. N. *Sov. J. Low Temp. Phys.* **1991**, *17*, 73.
(58) Silvera, I. F. *Rev. Mod. Phys.* **1980**, *52*, 393.
(59) Wang, X.; Andrews, L. *J. Phys. Chem. A* **2004**, *108*, 3396−3402.
(60) Grochala, W.; Edwards, P. P. *Chem. Rev.* **2004**, *104*, 1283.